minerals

MDPI

Article

Value Extraction from Ferrochrome Slag: A Thermochemical Equilibrium Calculation and Experimental Approach

Nilamadhaba Sahu [1,*], Gajanan U. Kapure [1], Pankaj Kumar [1], Sunil Kumar Tripathy [1,2,*], Arijit Biswas [1], Navneet Singh Randhawa [3] and Manas Paliwal [4]

[1] Research and Development, Tata Steel, Jamshedpur 831001, Jharkhand, India
[2] Natural Resources Research Institute (NRRI), University of Minnesota Duluth, Coleraine, MN 55722, USA
[3] Mineral Extraction and Forming Division, CSIR-National Metallurgical Laboratory, Jamshedpur 831007, Jharkhand, India; nsr@nmlindia.org
[4] Department of Metallurgical and Materials Engineering, Indian Institute of Technology Kharagpur, Kharagpur 721302, West Bengale, India; manas.paliwal@metal.iitkgp.ac.in
* Correspondence: nilamadhaba.sahu@tatasteel.com (N.S.); sunil@d.umn.edu (S.K.T.); Tel.: +1-218-256-4456 (S.K.T.)

Abstract: The valorization of slag from the production of high-carbon ferrochrome is a challenge for ferrochrome producers. The recycling of high-carbon ferrochrome slag was explored through the smelting route to recover Fe–Si–Al–Cr alloys and reengineer the residual slag for alumina-enriched refractory material. In this research, the focus was to reduce the SiO_2% and enrichment of Al_2O_3% in the final slag and recover the metallic value in the form of a complex alloy containing Fe, Si, Cr and Al. The manuscript consists of a thermochemical simulation of the smelting of FeCr slag followed by smelting experiments to optimize the process parameters such as temperature and the addition of coke, cast iron and alumina. An experimental investigation revealed that the maximum recovery of Si (57.4% recovery), Al in the alloy (20.56% recovery) and Al_2O_3 (85.78% recovery) in the slag was achieved at a charge mix consisting of 1000 g of FeCr slag, 300 g of alumina, 200 g of cast iron and 300 g of coke. The present study also demonstrated the usefulness of prior thermochemical calculations for smelting metallurgical wastes such as slag from high-carbon ferrochrome production for value creation and reutilization purposes.

Keywords: ferrochrome slag; valorization; FactSage; thermochemical equilibrium; smelting; refractory materials; high temperature

Citation: Sahu, N.; Kapure, G.U.; Kumar, P.; Tripathy, S.K.; Biswas, A.; Randhawa, N.S.; Paliwal, M. Value Extraction from Ferrochrome Slag: A Thermochemical Equilibrium Calculation and Experimental Approach. *Minerals* **2024**, *14*, 1097. https://doi.org/10.3390/min14111097

Academic Editor: Przemyslaw B. Kowalczuk

Received: 16 September 2024
Revised: 24 October 2024
Accepted: 28 October 2024
Published: 29 October 2024

1. Introduction

The high-carbon ferrochrome production process generates slag approximately 1.1–1.6 times that from alloy production. Naturally, the amount of generated slag is more than the amount of alloy produced. Currently, the majority of FeCr producers dump the slag or use it for landfilling purposes despite the little-known applications in construction activities as aggregates. This will create huge waste FeCr slag deposits over the years with the rising demand for FeCr production due to the increasing demand for stainless steel. A safe and economical solution for utilizing such a huge quantity of metallurgical waste is a serious challenge to ferrochrome producers due to the increasingly stringent environmental norms and the unavailability of storage space for the slag. Ferrochrome slag composition is close to refractory composition, and it contains 23%–25% spinel, 57%–68% forsterite and 1%–2% partially altered chromite (PAC) as refractory phases. The composition consists of 27 to 35 wt% of SiO_2, 15%–29% wt% of Al_2O_3, 23 to 33 wt% of MgO, 1 to 5 wt% of CaO, 7–13 wt% of Cr_2O_3 and FeO-1.8–5 wt% [1]. The melting temperature or refractoriness of ferrochrome slag can be increased by increasing the concentrations of MgO, Al_2O_3 and Cr_2O_3 separately or together. Therefore, various attempts were made to explore its utilization in refractory applications by modifying

its composition to the desired composition. Ashimov et al. developed forsterite-based refractory materials from ferrochromium slag [2]. Kumar et al. demonstrated the utilization of ferrochrome slag in refractory castables that can withstand up to 1300 °C [3]. Sahu et al. studied the development of high-temperature fused refractory materials containing refractory phases of forsterite, periclase and spinel from water-granulated ferrochrome slag through a sintering route [4]. Zhao et al. developed high-density refractory materials similar to brown fused alumina from aluminium–chromium slag produced from the aluminothermic smelting of chromite [5]. The above efforts explain the scope for utilizing FeCr slag in a refractory application by reengineering its composition to the desired application.

The experimental measurement of the smelting behaviour of oxide materials like ore or slag needs a lot of physical investigation. Hence, the thermochemical simulation of the smelting process using the available thermodynamic databases is quite useful for predicting the composition of slag, alloy and the off gas, slag liquidus temperature and alloy recovery. Hoe et al. used thermochemical calculations to predict the reduction behaviour of FeO in EAF slag during the aluminothermic smelting process [6]. Sarfo et al. used thermodynamics calculations to reduce the copper smelter slag in the presence of a carbon reductant and lime-alumina flux for recycling into pig iron and glass [7]. Zhang et al. used thermodynamics calculations and an experimental approach to study the recycling of nickel slag by using alumina dross [8]. Hamann et al. used thermochemical equilibrium calculations to examine the reduction of alumina to Al in the presence of methane or carbon under partial oxidation conditions and to predict the off-gas composition for designing the economical processing of it [9]. Though some prior studies indicated the usefulness of prior thermodynamics calculations applied to smelting metallurgical slags to recover metallic value from it, there is no literature available for similar attempts at smelting ferrochrome slag produced via high-carbon ferrochrome production. So, a proper investigation of the smelting process is required to explore its treatment in the downstream process. Therefore, any attempt to process the slag to recover the metal values and achieve complete utilization of the remaining materials after recovery will be helpful for these industries to recycle their waste for their sustainability. The current study was undertaken in the above direction.

The present study involved recycling high-carbon ferrochrome slag into Fe–Si–Al–Cr alloy and alumina-enriched refractory material through the carbothermal smelting process. In this research, the focus was to reduce the SiO_2% and enrichment of A_2O_3% in the final slag. The manuscript presents a thermochemical simulation of the smelting of FeCr slag followed by smelting experiments using FeCr slag to optimize the process parameters such as temperature along with the addition of coke, cast iron and alumina. The manuscript shows the usefulness of the prior thermochemical calculations for the smelting of metallurgical wastes such as slag from high-carbon ferrochrome production for value creation and reutilization purposes.

2. Materials and Methods

2.1. Thermochemical Simulation

The thermochemical equilibrium studies were conducted to decrease the SiO_2 and increase the Al_2O_3 content of FeCr slag via carbothermic reduction using a carbon reductant and the addition of alumina. Thermochemical simulations of the smelting of ferrochrome slag in the presence of a carbon reductant and iron were conducted using FactSage 7.2 databases to predict the possible extent of SiO_2 from slag under the simulation conditions explained later [10]. FactSage software and its thermodynamic database package were jointly developed by the Center for Research in Computational Thermochemistry (Quebec, Canada) and GTT-Technologies (Aachen, Germany). The reduction of SiO_2 from ferrochrome slag depends on (a) the temperature, (b) the amount of reductant, (c) alumina addition, and (d) iron addition. Thermochemical calculations were performed to optimize the carbon addition, Fe addition and Al_2O_3 addition using the FactSage equilib module with the FToxide, FactPs and FSstel databases for further experimental investigation. The chemical composition of the ferrochrome slag used in the simulation is presented in Table 1.

Table 1. Ferrochrome slag composition (wt%).

SiO_2	MgO	Al_2O_3	Cr_2O_3	Fe_2O_3	CaO	Cr (Metallic)
28.58	26.06	25.75	9.34	5.70	1.57	2.57

All the optimized processing conditions, such as the amount of coke addition, Fe addition and alumina addition, were used in the smelting experiments to investigate further the smelting behaviour of ferrochrome slag.

2.2. Smelting Experiments in a Submerged Arc Furnace

The experiments were planned based on the optimized conditions estimated through thermochemical simulation using FactSage. The chemical composition of the raw materials used in the experiments is shown in Table 2. All the raw materials, such as ferrochrome slag, coke, cast iron chips and alumina balls, were less than 5 mm in size. The chemical composition of ferrochrome slag and the slags obtained from the smelting tests was determined by combining the ASTM wet chemical [11] and instrumental methods [12]. About 100 gm of the representative sample was ground in a Vibratory Cup Mill to pass a 100-mesh BSS sieve. To analyze the metal sample obtained in the smelting tests, about 1 g of metal sample was dissolved in 50% (*v*/*v*) Hydrochloric acid (analytical grade, Merck) and diluted with ASTM grade I deionized water for analysis using an ICP-OES (iCAP7600, Thermo Fischer Scientific USA) calibrated using internal standard solutions. The charge composition of the material was prepared by mixing the calculated quantity of these raw materials based on thermodynamic equilibrium optimized conditions. So, the experiments were conducted with a smelting time of 50 min based on the above optimized conditions. Table 3 shows the composition of the charge mix for the smelting experiments. The experiments were planned based on a 1 kg FeCr slag treatment basis, and all the other input raw materials, such as coke, alumina and cast iron were considered as the weight percentages of the FeCr slag input. The charge mix for the experiments consisted of 1000 g of FeCr slag, 200 g (20 wt%) of cast iron, 300 g (30 wt%) of coke and 250–400 g (25–40 wt%) of alumina addition.

Table 2. Chemical compositions (wt%) of the raw materials.

Materials	Fe_2O_3	Cr_2O_3	SiO_2	CaO	MgO	Al_2O_3	Fixed Carbon	Volatile Material
FeCr slag	5.7	12.2	28.58	1.57	26.06	25.75	-	-
Coke	3.7	-	8.35	0.82	0.62	5.62	77.1	2.7
Alumina balls	-		0.4	-	-	99.5	-	-
	Fe		**Si**				**C**	
Cast iron chips	95.6		1.1				3.3	

Table 3. Composition of charge mix for the smelting experiments.

Expt. No	FeCr Slag (g)	Cast Iron (g)	Alumina (g)	Coke (g)	Smelting Time (Minutes)
1	1000	200	250	300	50
2	1000	200	300	300	50
3	1000	200	350	300	50
4	1000	200	400	300	50

The experimental setup for the smelting experiment shown in Figure 1 consists of a 50 kVA single-phase submerged arc furnace with a 50 kVA transformer unit. The furnace setup consists of a graphite crucible (2 kg capacity), graphite electrode (diameter of 50 mm), electrode holding arm–column assembly, graphite base plate and refractory-lined shell. The bottom plate and the refractory-lined surface around the graphite crucible support the graphite crucible. The top cover of the crucible consists of a refractory-lined lid with a hole

in the middle for electrode movement. A pair of water-cooled brass clamps for holding the electrode is mounted on the electrode-holding arm. The electrode-holding arm is attached to a column, and the electrode arm–column assembly can move in a vertical direction to position the electrode at the desired level via manual operation. During operation, the phase and neutral points of the AC power source are connected to the electrode and base carbon plate, respectively.

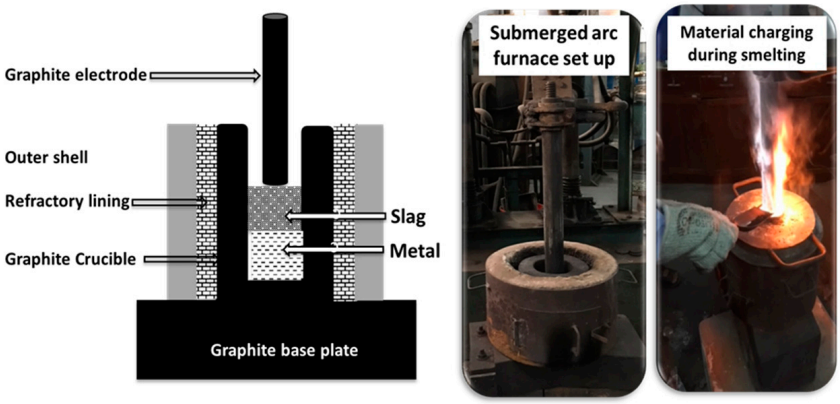

Figure 1. Experimental setup for smelting studies.

In all the smelting experiments, the operation time consists of preheating the crucible, feeding raw material into the crucible, and soaking or holding under the continued arcing condition as per the requirement of the experiment. For preheating purposes, a few pieces of coke were placed at the bottom of the crucible, and the electrode was lowered for arcing. The preheating of the crucible (by arcing between the electrode and coke) continued till the crucible became red-hot. The feeding of raw materials into the red-hot crucible started after the preheating operation. The raw material mix was introduced into the crucible slowly in small quantities until a sufficient molten pool was generated by melting the initial charge mix. The arcing continued to raise the temperature of the molten bath further under the high-temperature arcing zone. Though there was no control of the temperature under the influence of the arcing, the molten bath temperature during the experiments was maintained sufficiently high through downward electrode movement, so a molten pool was maintained in the crucible during the experiments. The charging operation was completed in 35 min. After charging, the arcing operation continued for 15 more minutes. So, the smelting operation was continued for 50 min, including feeding and after feeding. The electrode was completely withdrawn from the crucible after the completion of the smelting operation. The slag–metal molten mass pool was left inside the crucible for cooling. After cooling, the cooled slag–metal mass was removed from the crucible, and the slag and metal were separated manually.

2.3. Mineralogical Analysis

X-ray diffraction analysis and scanning electron microscopic image analysis were carried out for the slag samples obtained after the smelting experiments to investigate the presence of refractory phases in it. The specimens for the SEM investigation were prepared via cold mounting followed by polishing and a thin layer of carbon coating of the polished surface. The SEM investigations of the slag samples were carried out using a JOEL JXA-8230 electron probe microanalyzer.(Tokyo, Japan) The X-ray diffraction investigation for the powder slag samples was carried out with a PANalytical X'Pert PRO X-ray diffractometer using CuKα radiation in the 2θ range from 10° to 90°. The possible mineral phases were identified by using PANalytical HighScore plus XRD analytical software (Version. 3.0d (3.0.4)).

3. Results

3.1. Thermo-Chemical Simulation of Smelting of FeCr Slag to Understand SiO_2 Reduction Using the Thermodynamics Database in FactSage

For the optimization of carbon addition during the smelting of ferrochrome slag, thermodynamic calculations were performed in the presence of carbon alone at temperatures varying from 1600 to 2400 °C. The addition of carbon was varied from 10 wt% to 50 wt% of FeCr slag with a variation in temperatures from 1600 °C to 2400 °C as below (Equation (1)):

FeCr slag + <10–50 wt%> carbon; temperature: 1600–2400 °C (1)

For the optimization of the Fe addition during the smelting of ferrochrome slag, the calculations were performed at an Fe addition of 0 to 50 wt% of FeCr slag, keeping the carbon addition fixed at 25 wt% of FeCr slag at 1600–2400 °C as below (Equation (2)):

FeCr slag + 25 wt% carbon + <0–50 wt%> Fe; temperature: 1600–2400 °C (2)

For the optimization of the alumina addition during the smelting of ferrochrome slag, the calculations were performed at an Al_2O_3 addition of 0 to 50 wt% of FeCr slag, keeping the carbon and iron addition fixed at 25% and 20% of FeCr slag, respectively, at temperatures of 1600–2400 °C as below (Equation (3)):

FeCr slag + 25 wt% carbon + 20 wt% Fe + <0–50 wt%> Al_2O_3; temperature: 1600–2400 °C (3)

3.1.1. Effect of Carbon Addition

The SiO_2 reduction from FeCr slag by carbon can be represented by Equation (4), as given below. However, the literature explains the mechanism of the carbothermic reduction of SiO_2 via the formation of SiO (g) and SiC as intermediate products. The related intermediate equations showing the formation of SiO (g) and SiC are presented in Appendix A as Equations (A1)–(A8) [13].

$$SiO_2\ (l) + 2C\ (s) = Si\ (l) + 2CO\ (g);\ \Delta G^0 = 685.34 - 0.352\ T\ (kJ) \quad (4)$$

Figure 2 shows the predicted equilibrium SiO_2 composition map for the slag after the smelting of ferrochrome slag for the variation in carbon addition (10–50 wt% of FeCr slag) at different temperatures (1600–2400 °C). The SiO_2 contour map is useful for identifying the optimum smelting window for the carbon addition and smelting temperature for maximum SiO_2 reduction from FeCr slag leading to minimum amounts of SiO_2 in the final slag. The optimum conditions with respect to the carbon addition and smelting temperature for <5 wt% SiO_2 in the final slag are shown as hatched lines on the SiO_2 contour map. The SiO_2 reduction is not significant at 1600–1700 °C. It is clearly evident that the effect of a carbon reductant on the reduction of SiO_2 is significant till a 25 wt% carbon addition at all temperatures above 1800 °C. The variation in SiO_2 content in the final slag can be best understood with the help of the variation in the equilibrium distribution of Si between the slag and alloy. The equilibrium Si partition ratio is calculated as the ratio of wt% of Si in slag to wt% of Si in the alloy, as shown in Figure 3. The predicted equilibrium Si partition ratio curve at 1600 °C remains almost flat with a variation in carbon addition as the variation in carbon has a negligible impact on the reduction of SiO_2 at this temperature. The predicted equilibrium Si partition ratio curves decrease till a 25 wt% carbon addition, remain almost constant thereafter in the lower temperature range (1700–1900 °C) and increase slightly up to a 35 wt% addition before saturation at higher temperatures (2000–2400 °C).

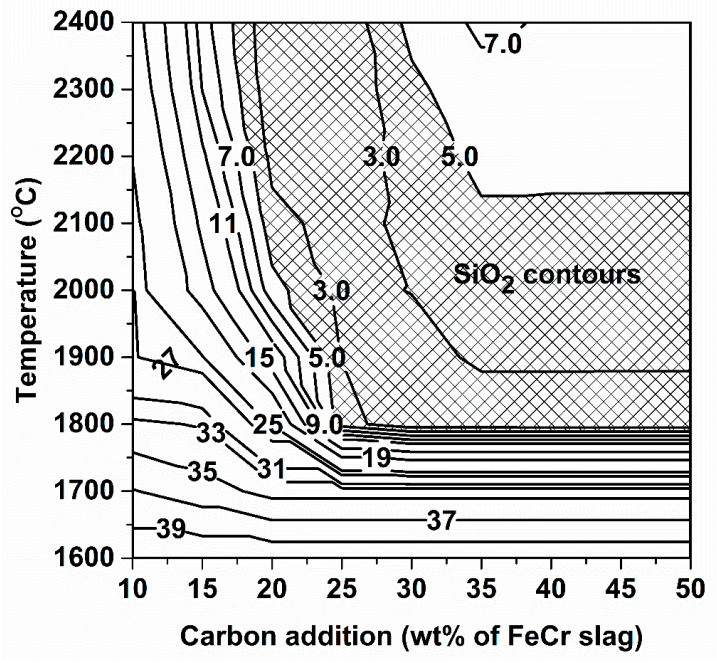

Figure 2. Variation in predicted SiO_2 (wt%) map for slag with carbon addition at different temperatures.

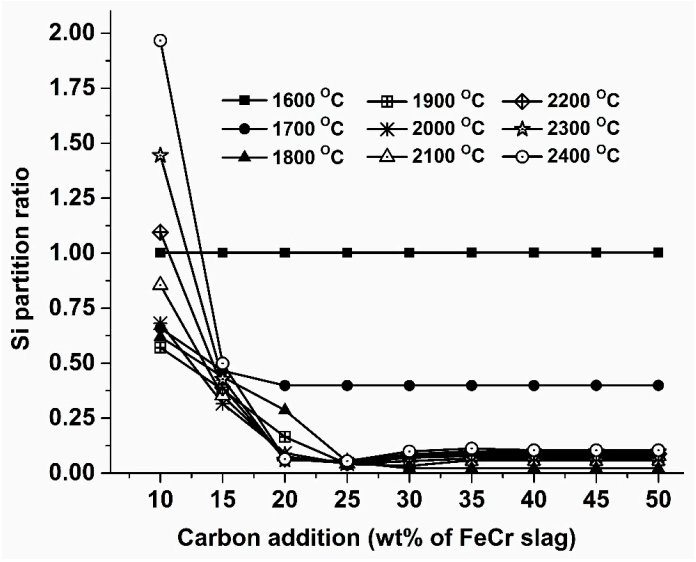

Figure 3. Variation in predicted Si partition ratio with carbon addition at different temperatures.

Based on this simulation study, it was decided to fix the carbon addition at 25 wt% in the subsequent simulation studies to identify the various other process parameters.

3.1.2. Effect of Fe Addition on the SiO_2 Reduction

The SiO_2 reduction from FeCr slag in the presence of Fe can be represented by the following Equation (5):

$$SiO_2\ (l) + 2C\ (s) + Fe\ (l) = FeSi\ (l) + 2CO\ (g);\ \Delta G^0 = 603.1 - 0.3444\ T\ (kJ) \quad (5)$$

The reduction of SiO_2, as per Equation (5) can be feasible at a much lower temperature (T > 1478 °C) compared to that of Equation (4) (T > 1673 °C). The purpose of the Fe addition is to lower Si's activity in the alloy and thereby increase the activity of SiO_2 in the molten slag to favour the carbothermic reduction of SiO_2. The effect of the Fe addition on the SiO_2 reduction was studied assuming a 25 wt% carbon addition as an optimized quantity

of reductant described earlier. Figures 4 and 5 explain the variation in the predicted equilibrium SiO_2(wt%) in the slag and predicted equilibrium Si recovery (%) in the alloy with a variation in Fe addition, respectively. An Fe addition has a minimal effect on reducing the SiO_2 percentage above 1800 °C. However, a significant effect of an Fe addition on SiO_2 reduction is observed below 1800 °C. The predicted SiO_2(wt%) in the slag decreases with increasing Fe addition at 1600 °C and 1700 °C, but at 1800 °C, the SiO_2(wt%) decreases up to a 20 wt% Fe addition and increases thereafter. The equilibrium SiO_2(wt%) in the slag during the smelting of FeCr slag can be understood with the help of the variation in the predicted Si recovery in the alloy at equilibrium. The predicted Si recovery increases with increasing Fe addition at all temperatures. The predicted equilibrium Si recovery in the alloy increases from 1600 °C to 1800 °C and decreases thereafter with increasing temperature for all levels of Fe addition. The recovery of Si in the alloy is predicted to be at the maximum at 1800 °C for all levels of Fe addition. The variation in SiO_2 percentage in the slag and Si recovery in the alloy can be explained with the help of the equilibrium activity of Si in the alloy and the equilibrium partial pressure of SiO in the gas phase. The equilibrium Si activity in the alloy decreases with increasing Fe addition at all temperatures, which increases the activity of SiO_2 during smelting. The equilibrium partial pressure of SiO in gas decreases with increasing Fe addition, which is also related to a higher Si recovery in the alloy by decreasing the Si loss in the form of SiO in gas. The decreasing Si recovery in the alloy with increasing temperature above 1800 °C is attributed to the higher Si loss in the gas phase with increasing temperature. The reason for this may be due to the fact that the carbothermic reduction of SiO_2 at a lower temperature (<1800 °C) occurs mostly inside the molten slag, but a part of the SiO_2 reduction occurs via the formation of SiO (g) vapour at high temperatures (>1800 °C). Increasing the Fe addition decreases the percentage of Si and Cr in the final alloy, therefore degrading the quality of the final ferroalloy produced. So, considering the above discussion, Fe addition at 20 wt% of FeCr slag was considered for the subsequent studies.

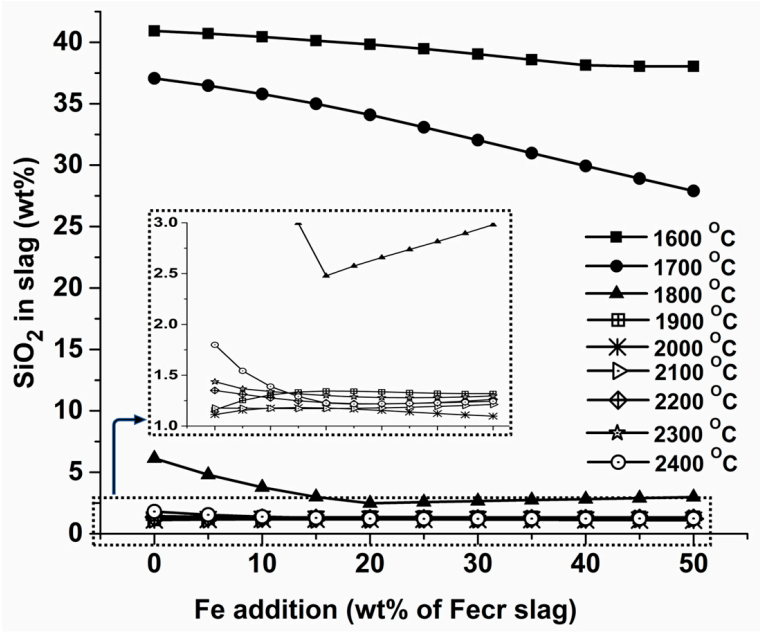

Figure 4. Variation in predicted SiO_2 (wt%) with Fe addition.

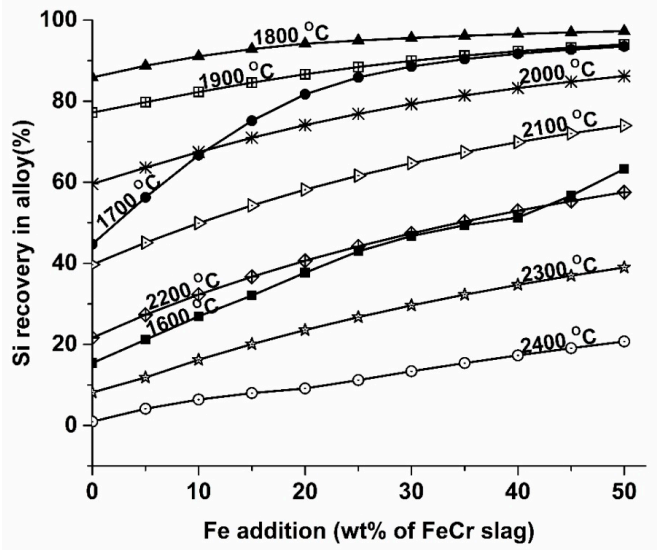

Figure 5. Variation in predicted Si recovery(%) in alloy with Fe addition.

3.1.3. Effect of Al_2O_3 Addition on the SiO_2 Reduction

The effect of Al_2O_3 addition on the SiO_2 percentage in the slag was studied considering a 25 wt% carbon and 20 wt% Fe addition, as discussed above. The purpose of adding Al_2O_3 during smelting is to decrease the SiO_2(wt%) in the final slag and enrich the Al_2O_3-containing phases, such as spinel and alumina, in the final slag. Figure 6 shows the predicted SiO_2(wt%) variation with Al_2O_3 addition at different temperatures. Al_2O_3 addition has almost no effect on decreasing the SiO_2(wt%) in the slag till a 35 wt% Al_2O_3 addition at 1600 °C. However, with a higher amount (>35 wt%) of Al_2O_3 addition at this temperature, the SiO_2(wt%) in the slag decreases. Similarly, at 1700 °C, the SiO_2(wt%) in the slag decreases after a 25 wt% Al_2O_3 addition. The addition of Al_2O_3 has a negligible effect on decreasing the SiO_2(wt%) in the slag at higher temperatures (1800–2400 °C). The impact of Al_2O_3 addition on the SiO_2 reduction can also be understood via the variation in the Si recovery trend in the alloy with the Al_2O_3 addition shown in Figure 7. The predicted Si recovery in the alloy increases significantly with increasing Al_2O_3 addition at lower temperatures (1600–1700 °C) and remains constant or increases insignificantly at higher temperatures (1800–2400 °C).

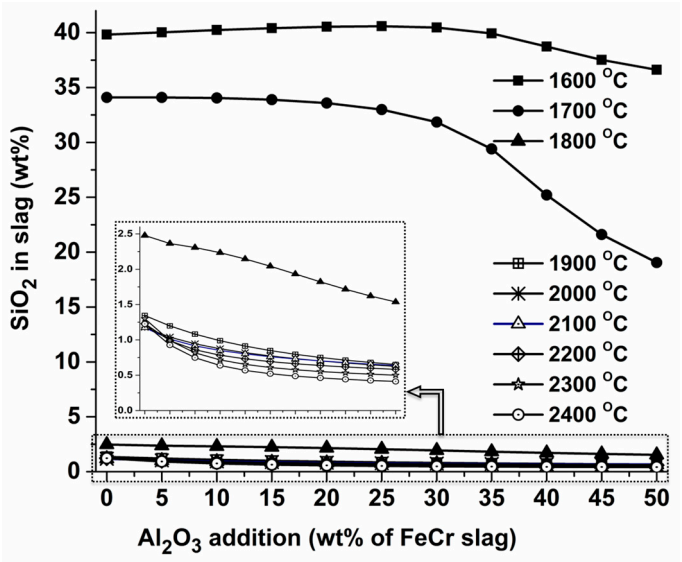

Figure 6. Predicted variation in SiO_2 (wt%) with Al_2O_3 addition at different temperatures.

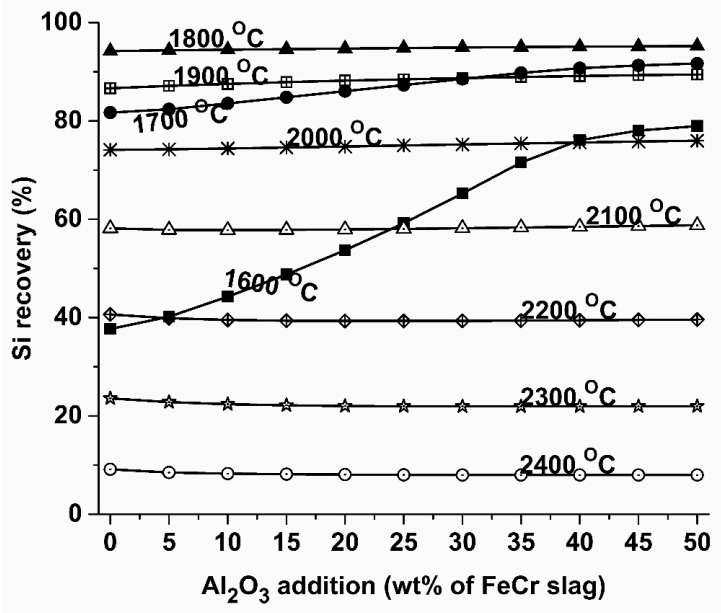

Figure 7. Predicted variation in Si recovery in alloy with Al_2O_3 addition at different temperatures.

3.2. Smelting of FeCr Slag in a Submerged Arc Furnace

The thermochemical simulation of the smelting of FeCr slag indicated an optimized quantity of carbon addition (25 wt% of FeCr slag) and Fe addition (20% of FeCr slag) for the reduction of SiO_2 from FeCr slag. The simulation also indicated that a significant reduction of SiO_2 from slag can happen beyond a 25% Al_2O_3 addition at lower temperatures. Further experiments were conducted under the above optimized conditions of Fe (20 wt% of FeCr slag) and carbon (25 wt% of FeCr slag) with a variation in alumina (25%–40% of FeCr slag) to check the feasibility of the recovery of the value from FeCr slag through smelting. The experiments were repeated twice for similar testing conditions for the consistency of the experimental outcome and the average results are presented. The variation in the results such as the composition of the alloy, slag and their recoveries were less than 5%. The smelting experiments yielded two products: (1) the Fe–Si–Cr–Al alloy and (2) the high Al_2O_3-containing slag. The slag and alloy compositions and their recovery obtained after the smelting experiments are presented in Tables 4 and 5, respectively.

Table 4. Experimental slag composition and recovery.

Expt No	Slag Composition (wt%)						Slag Recovery (%)		
	Al_2O_3	MgO	SiO_2	Cr_2O_3	CaO	Fe_2O_3	Al_2O_3	MgO	SiO_2
1	65.42	8.28	11.52	1.3	6.72	2.95	80.16	20.22	23.67
2	70.71	6.27	7.94	2.0	5.73	4.15	85.78	16.60	17.68
3	70.72	8.82	7.28	1.19	5.42	2.54	77.69	22.98	15.94
4	76.45	5.61	5.77	1.64	5.51	3.34	84.36	15.86	13.70

Table 5. Experimental alloy composition and recovery.

Expt No	Alloy Composition (wt%)				Alloy Recovery (%)		
	Si	Cr	Al	C	Si	Cr	Al
1	21.17	16.85	15.37	2.65	51.69	73.90	20.32
2	22.24	15.11	16.19	2.28	57.24	69.71	20.56
3	20.58	15.35	12.32	3.86	56.63	75.78	15.41
4	22.09	16.16	13	2.12	55.86	73.39	13.85

Figure 8 shows the variation in the composition of the slag obtained after the smelting experiments of FeCr slag. The SiO_2(wt%) in the slag decreases from 11.52% to 5.77% with increasing alumina addition from 25 wt% to 40 wt%. Similarly, the Al_2O_3 (wt%) in the slag increases from 65.42% to 76.45% with increasing alumina addition from 25 wt% to 40 wt%. Figure 9 shows the variation in the recovery of Al_2O_3, MgO and SiO_2 in the slag with alumina addition. The Al_2O_3 recovery in the slag ranges from 77.69 to 85.78% for an alumina addition of 25–40 wt%. The highest Al_2O_3 recovery (85.78%) in the slag is observed at a 30 wt% alumina addition. The SiO_2 recovery in the slag decreases due to the increasing carbothermic reduction of SiO_2 with increasing alumina addition. The MgO recovery in the slag ranges from 15.86 to 22.98%, and the lower MgO recovery is due to MgO loss in the form of Mg (g). The slag recovery is mainly affected by gas phase losses in the form of Mg(g), Al_2O(g) and SiO(g). These gaseous products become oxidized while leaving the furnace, and a part of them is deposited as dust on the furnace cover and the upper part of the electrode. The variation in the composition of dust with alumina addition is presented in Figure 10 and Table 6. The MgO(wt%) in dust increases with increasing alumina addition from 25 wt% to 40 wt% as the partial pressure of Mg(g) increases with the increasing activity of Al_2O_3. The Al_2O_3 (wt%) in dust follows the opposite trend of SiO_2(wt%) with increasing alumina addition from 25 wt% to 40 wt% addition as the partial pressure of Al_2O(g) and SiO(g) are related indirectly. The dust with the composition of MgO: 36.1–43.6%, Al_2O_3: 19.8–25.03% and SiO_2: 15.41–18.02% was collected after the experiments. The dust containing the lowest Al_2O_3 of 19.8% and the highest SiO_2 of 18.02% is observed at a 30 wt% alumina addition. Therefore, the addition of 30 wt% alumina can be used as an optimum condition for Al_2O_3% enrichment in the slag, considering its recovery in the slag and loss in the dust. The high alumina slag obtained after the smelting experiments can be used as raw materials in refractory applications.

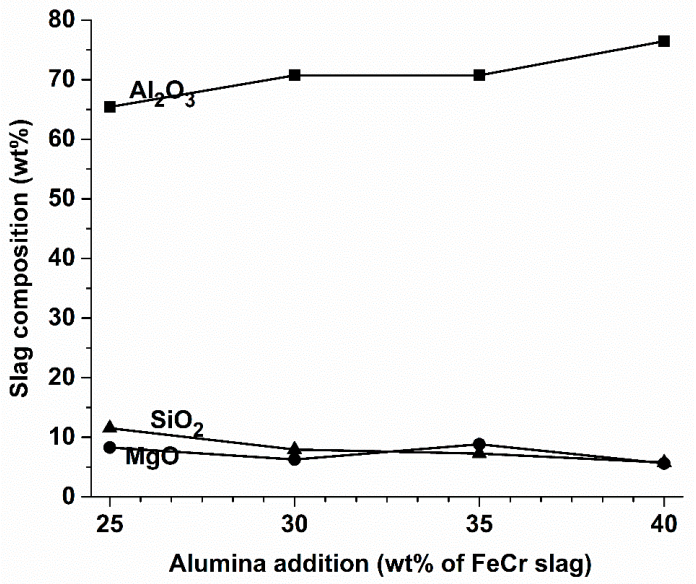

Figure 8. Variation in experimental SiO_2 (wt%) and Al_2O_3 (wt%) in slag with alumina addition.

Table 6. Experimental dust composition (in wt%).

Expt No	Al_2O_3	SiO_2	MgO	Cr_2O_3	CaO	Fe_2O_3
1	25.03	15.41	36.1	2.34	3.65	7.57
2	19.8	18.02	41.95	2.16	2.89	3.97
3	22.2	16.52	40.35	11	3.16	4.13
4	21.7	17.45	43.65	2.12	3.04	4.60

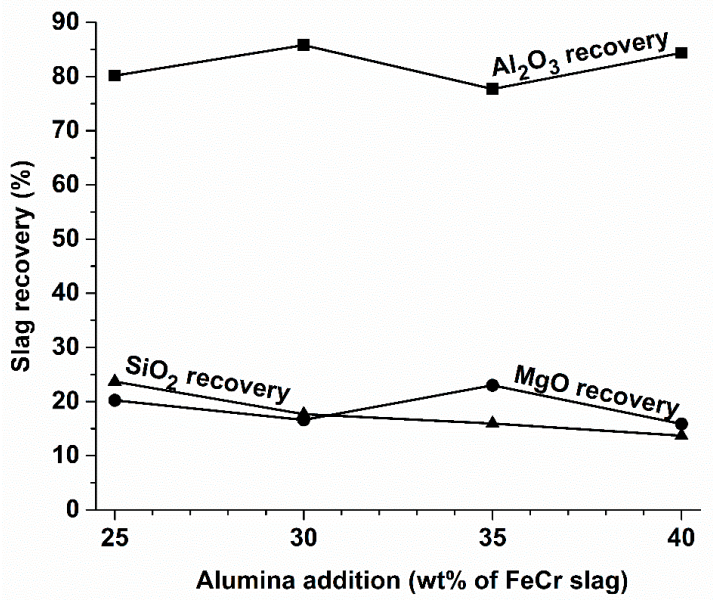

Figure 9. Variation in experimental slag recovery with alumina addition.

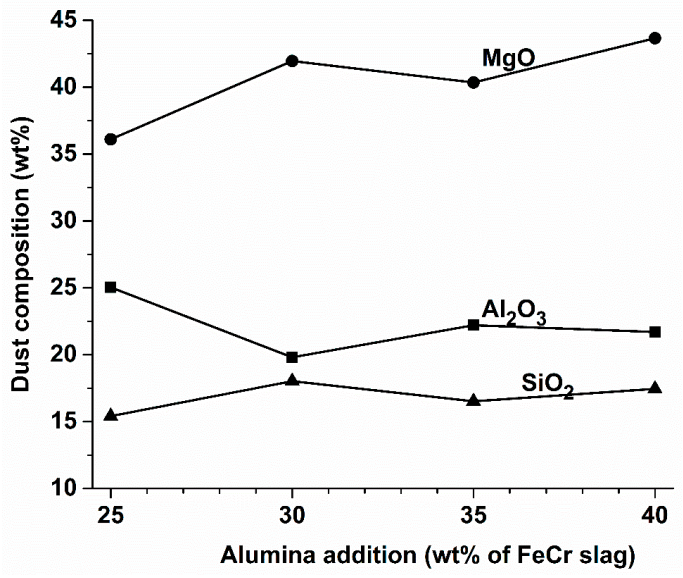

Figure 10. Variation in experimental dust composition (wt%) with alumina addition.

The experimental alloy composition and recovery obtained after the smelting of FeCr slag are shown in Figures 11 and 12. An alloy containing Si: 20.58%–22.24%, Al: 12.32%–16.19% and Cr: 15.11%–16.85% was produced with an alumina addition from 25 wt to 40 wt%. The oxides such as Cr_2O_3 and SiO_2 were reduced to their respective metallic form by the carbon reductant in the presence of iron and joined the alloy pool. The Cr_2O_3 present in the slag was reduced to Cr as per the following Equation (6) and joined the alloy pool. In fact, the carbothermic reduction of Cr_2O_3 will be more favoured in the presence of a molten iron alloy pool by reducing the activity of the Cr in the alloy.

$$Cr_2O_3 + 3C = 2Cr + 3CO;\ \Delta G^\circ = 700.581 - 0.4821T\ (kJ) \quad (6)$$

The presence of Al in the alloy composition indicates that a part of the input Al_2O_3 of the charge mix was reduced by the carbon reductant in the presence of the molten iron alloy during the smelting. The low-temperature carbothermic reduction of alumina in the presence of iron was also reported by Khanna et al., 2016 [14]. The low-temperature

(1550 °C) reduction of alumina can occur through the formation of gaseous suboxide Al_2O as represented by the following reaction sequences:

$$Al_2O_3 \xrightarrow{C} Al_2O \xrightarrow{C} Al \xrightarrow{Fe,C} Fe-Al; Fe-Al-C$$

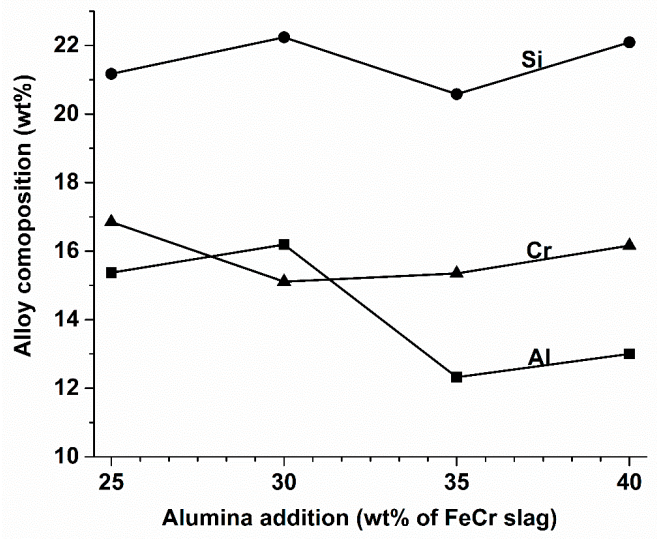

Figure 11. Variation in alloy composition (wt%) with alumina addition.

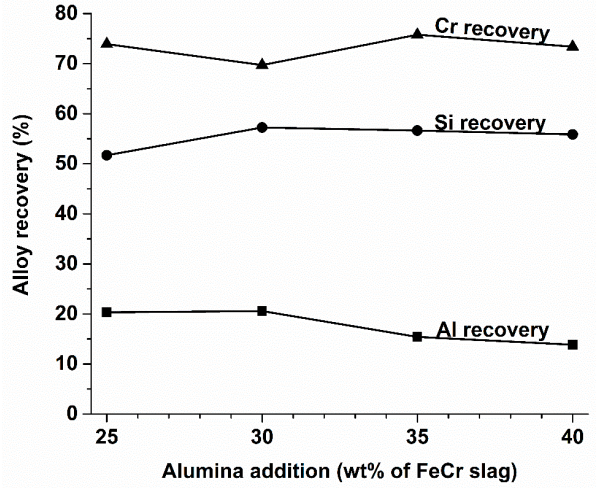

Figure 12. Variation in alloy recovery (%) with alumina addition.

Similarly, the low-temperature reduction of SiO_2 during smelting is also favoured in the presence of an iron alloy pool, as per Equation (5) described earlier. The recovery in the alloy follows the order of Cr recovery > Si recovery > Al recovery as the ease of reduction of their oxides during smelting is in the order of $Cr_2O_3 > SiO_2 > Al_2O_3$. The variation in Si wt% and Si recovery curves follows a similar trend with a variation in Si wt% and Si recovery curves following a similar trend with the addition of alumina from 25 wt% to 40 wt%. However, the Cr wt% and Cr recovery curve follow opposite to that of the Si and Al from 25 wt% to 35 wt% alumna addition. The variation in the alloy percentage and recovery curves for Cr, Si and Al follows the same trend as from 35 wt% to 40 wt% alumina addition. All the alloy recovery curves seem to be flat from 35 wt% to 40 wt% alumina addition. This indicates that the maximum reduction of oxides is achieved till a 40 wt% alumina addition, and there may not be any appreciable change in the alloy recovery over a 40 wt% alumina addition. The variation in the alloy percentage and alloy recovery with the addition of 25 wt% to 40 wt% alumina can be explained by the slag metal equilibrium reactions involving the reduction of Cr_2O_3 and SiO_2, as shown in Equation (7).

$$2Cr_2O_3 + 3Si = 4Cr + 3SiO_2;\ \Delta G^\circ = -730 + 0.133\ T\ (kJ) \quad (7)$$

The equilibrium constant Keq2 for Equation (7) can be expressed as Equation (8) as follows:

$$K_{eq2} = \frac{(a_{SiO_2})^3.(a_{Cr})^4}{(a_{Cr_2O_3})^2.(a_{Si})^3} \quad (8)$$

The highest recovery of 57.4% of Si and 20.56% of Al in the alloy was observed at a 30 wt% alumina addition with concentrations of Si: 22.24 wt%, Al: 16.19 wt% and Cr: 15.11 wt% in the alloy.

3.3. Phase Analysis of the Slag After the Smelting

The X-ray diffraction analysis of the high alumina slag samples obtained after the smelting experiments is shown in Figure 13. The X-ray diffraction analysis of the slag samples revealed the presence of phases such as spinel, aluminium oxide, calcium aluminium oxide and forsterite. The peaks for the forsterite phase are visible prominently in the lower alumina (25 wt% and 30 wt%) additions. However, these silicate phases are not prominent for the higher alumina additions (35 wt% and 40 wt%). Similarly, the aluminium oxide phases emerge prominently at higher alumina additions than lower alumina additions.

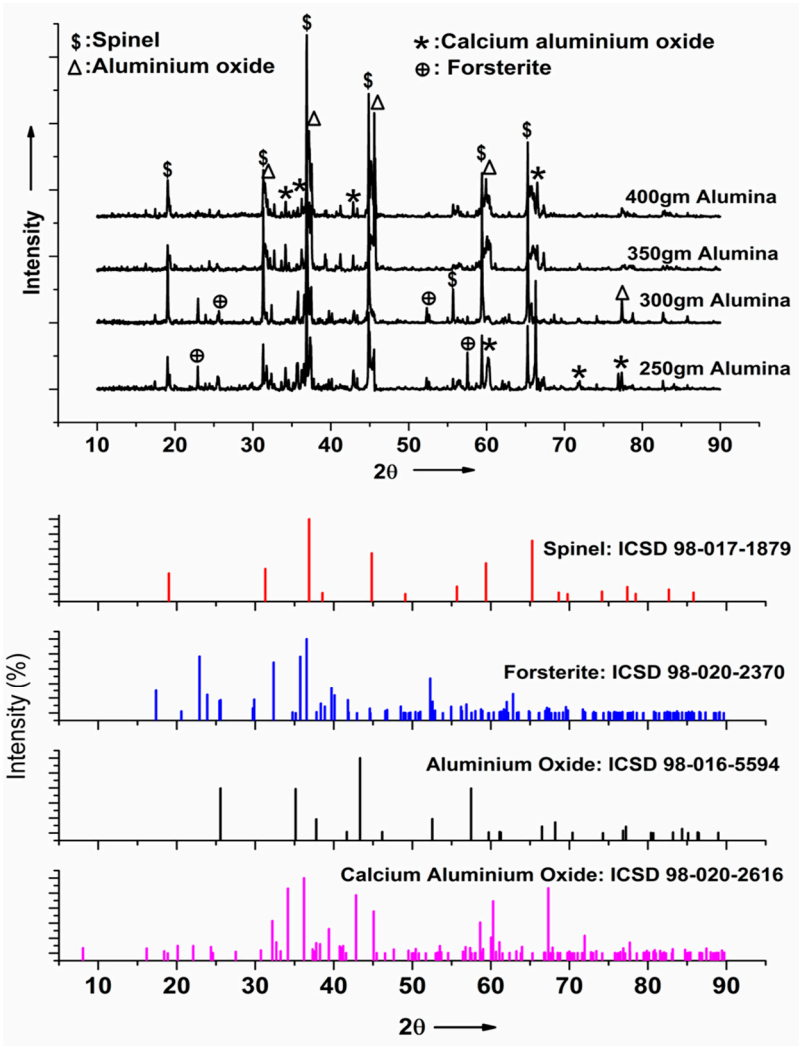

Figure 13. XRD analysis of slag samples obtained after smelting.

Figure 14 presents the SEM micrograph of the slag samples obtained after the smelting experiments. All the SEM micrographs of the slag samples contain dark, grey, bright and brightest phases. The dark phases belong to alumina-rich spinel phases ($MgAl_2O_4$ and Al_2O_4), grey phases belong to alumina-rich calcium aluminate phases ($CaAl_{12}O_{19}$), bright phases belong to glassy phases containing CaO-Al_2O_3-SiO_2 and brightest phases belong to metallic entrapments. The XRD and SEM analysis revealed that the spinel ($MgAl_2O_4$) and aluminium oxide (Al_3O_4) phases are the major crystal structures in all the slag samples, and the calcium aluminosilicate glassy phases present as the minor phase. The calcium aluminosilicate phase is distinctly visible along with other phases, such as the calcium aluminate and spinel phases, in the SEM micrograph of the slag obtained from experiment 1. The calcium aluminosilicate phase diminishes in the SEM micrographs of the slag obtained from experiments 2,3, and 4. The micrographs of the slag obtained from experiments 2, 3 and 4 show more prevalence of alumina-rich phases such as calcium aluminate and spinel phases compared to the slag obtained from experiment 1. The appearance of the calcium aluminosilicate glassy phase in the SEM micrograph decreases, with increasing alumina addition. The fused slag obtained after the smelting may have a refractory application due to the presence of major refractory phases such as spinel ($MgAl_2O_4$ and Al_3O_4) and calcium aluminate ($CaAl_{12}O_{19}$) [15–17].

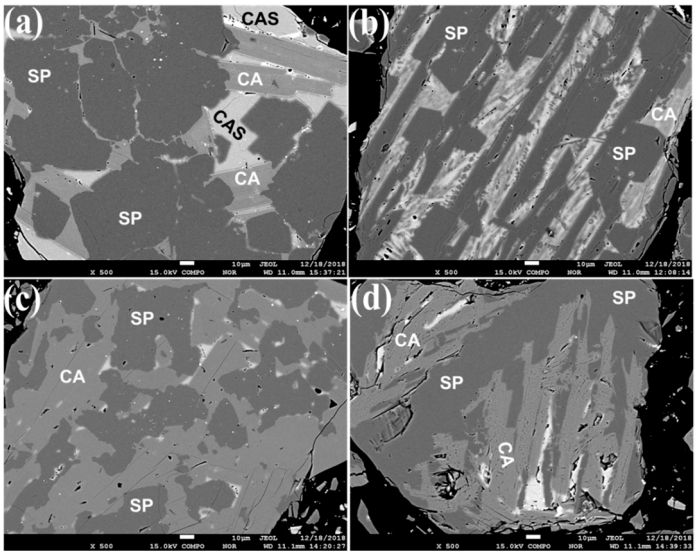

Figure 14. SEM analysis of slag after smelting experiments ((**a**–**d**) for experiments 1 to 4); SP: spinel, CAS: calcium aluminosilicate, CA: calcium aluminate.

4. Discussion

During the smelting of ferrochrome slag in a submerged arc furnace to produce high alumina fused refractory slag and the Fe–Si–Cr–Al alloy, various process parameters affect the final product's quality and recovery. As discussed earlier, the different process parameters were optimized using thermochemical calculations followed by the smelting experiments. The optimized smelting conditions for the production of fused refractory slag and the Fe–Si–Cr–Al alloy from ferrochrome slag are visually summarized in Figure 15. A higher recovery of Al_2O_3 and lower recovery of SiO_2 is preferred for refractory products and quality. Hence, a lower Al recovery and higher Si recovery are preferred in alloys, along with a higher Cr recovery. The most preferred optimized charge composition for the production of high alumina refractory slag and the Fe–Si–Cr–Al alloy during the smelting of ferrochrome slag is the addition of 30% of coke, 20% of cast iron and 40% of alumina.

Figure 15. Summary of the smelting experiments for production of fused refractory and Fe–Si–Cr–Al alloy from ferrochrome slag.

The composition of the alloy with this most preferred charge composition consists of Si-22.09 wt%, Cr-16.16 wt%, Al-13 wt% and C-2.12 wt% with the recovery of Si, Cr and Al in the alloy of 55.86%, 73.39% and 13.85%, respectively. The composition of high alumina refractory slag with the most preferred charge composition consists of Al_2O_3-76.45 wt%, MgO-5.61 wt%, SiO_2-5.77 wt% and Cr_2O_3-1.64 wt% with the recovery of Al_2O_3, MgO and SiO_2 of 84.36%, 15.86% and 13.7%, respectively. The complex ferroalloy containing iron, silicon, chromium and aluminium obtained after the smelting of FeCr slag can be used in the production of low- and medium-carbon ferrochrome and for stainless steel making [18–21].

Zero-waste ferrochrome production could be possible if the metallic value is extracted as an alloy from the molten ferrochrome slag and the remaining slag is re-engineered into a refractory raw material composition for further use in refractory making. The temperature of the molten ferrochrome slag during tapping is around 1650–1750 °C. Hence, to utilize the energy contained in the molten ferrochrome slag, the current research proposes to use the molten ferrochrome slag as the starting raw material for metallic value extraction and slag reengineering to produce fused refractory material.

5. Application of the Current Slag Towards Tap-Hole Clay Formulation

In order to drain out the hot metal from the blast furnace, the tap-hole clay has to be drilled through and then plugged again after the completion of the tapping process. The tap-hole clay must have good refractory properties and high-temperature strength as it is exposed to hot metal and slag at high temperatures and pressure in the blast furnace. Thus, the clay's quality needs to be high to increase the blast furnace's productivity. Typically, tap-hole clay consists of a matrix phase, filler (generally coke), binder, resin, high-temperature phase, which could be similar to a matrix phase, and an abrasive phase such as SiC or SiN. In this section, we are going to utilize the final fused slag composition and demonstrate its effectiveness as tap-hole clay. The fused slag composition obtained after experiment no. 4 was selected as a starting point for the design of the tap-hole clay. SiC was chosen as an abrasive phase, and a certain amount of C was added to the mix to obtain the final clay composition. The final optimized clay composition is mentioned in Table 7, along with a typical blast furnace slag composition. It is noted that 18 wt% of SiC was added as an abrasive phase, and 4 wt% of C is assumed to be a volatile material. The slag and clay interaction calculations are summarized in Figure 16 for 1600 °C. As seen, the 0 and 100 on the *X*-axis refer to the 100% slag and 100% clay formulations at 1600 C. It is reasonable to consider that the real interactions under the actual operating conditions will occur close to the clay composition. It is seen that when the interactions are captured close to the clay composition (90% clay and 10% slag), around 40.12 g of calcium magnesium aluminate phases, 24.38 g of calcium aluminate phases and 7.34 gm of spinel phases are formed, which are high-temperature refractory phases and are expected to provide good high-temperature corrosion resistance. In addition, 17.27 g of SiC is retained in the mixture in comparison to the 16.76 g (present at the 90% formulation) and no molten slag. This suggests that there is the thermodynamic possibility of in situ SiC formation as C can reduce the SiO_2

in the BF slag and form SiC. The Al_2O_3, CaO and MgO constituents in the tap-hole clay formulation form high-temperature phases such as calcium magnesium aluminate, calcium aluminate phases and spinel. From the above calculations, it is demonstrated that the current fused slag composition obtained after the SAF experiments can be utilized as a tap-hole clay formulation. Further optimization of SiC and C addition can be performed along with controlled interaction experiments to validate the feasibility of this slag as a tap-hole clay material.

Table 7. Blast furnace tap-hole clay and blast furnace slag composition.

Optimized Tap-hole Clay Composition	Al_2O_3	MgO	SiO_2	Cr_2O_3	CaO	Fe_2O_3	SiC	C
	63.54	4.66	4.80	1.36	4.58	2.78	14.96	3.32
Typical Blast Furnace Slag Composition	Al_2O_3	MgO	SiO_2	MnO	CaO			
	17.5	10	34	3.5	35			

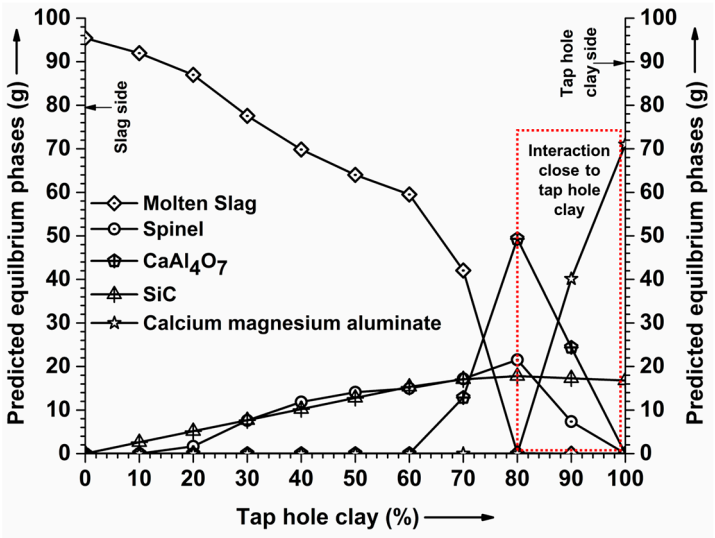

Figure 16. Summary of blast furnace slag and tap-hole clay predicted thermodynamics interaction at 1600 °C.

6. Conclusions

The recycling of high-carbon ferrochrome slag is explored through the smelting route to recover the Fe–Si–Al–Cr alloy and reengineer the residual slag for alumina-enriched refractory material. The following conclusions are summarized.

- The thermochemical calculations using the available thermodynamic databases and laboratory-scale smelting experiments indicated that ferrochrome slag, which is a waste byproduct of high-carbon ferrochrome production, can be converted to two products such as high Al_2O_3-containing refractory material and a complex ferroalloy of Fe–Si–Cr–Al.
- The thermochemical simulation of the smelting of high-carbon ferrochrome slag predicted the optimum process parameters such as the temperature, amount of the carbon reductant, iron addition and Al_2O_3 addition for reengineering the slag composition to achieve low SiO_2 and high Al_2O_3 slag with the optimum recovery of the metallic value from it.
- An experimental investigation revealed that the optimized charge composition for the smelting of ferrochrome slag is the addition of 30% of coke, 20% of cast iron and 40% of alumina.

- The composition of the complex ferroalloy produced during the optimized smelting conditions consists of Si-22.09 wt%, Cr-16.16 wt%, Al-13 wt% and C-2.12 wt% with the recovery of Si, Cr and Al in the alloy of 55.86%, 73.39% and 13.85%, respectively.
- The composition of the high Al_2O_3-containing refractory material produced during the optimized smelting condition consists of Al_2O_3-76.45 wt%, MgO-5.61 wt%, SiO_2-5.77 wt% and Cr_2O_3-1.64 wt%. The recoveries of Al_2O_3, MgO, and SiO_2 are 84.36%, 15.86%, and 13.7% of the product during smelting.
- The high Al_2O_3-containing refractory material produced after the smelting contains spinel ($MgAl_2O_4$ & Al_3O_4) and calcium aluminate ($CaAl_{12}O_{19}$) as a major refractory phase.

Author Contributions: Conceptualization, N.S., S.K.T. and G.U.K.; methodology, N.S., P.K. and N.S.R.; software, N.S., A.B. and M.P.; validation, N.S., P.K., A.B. and G.U.K.; formal analysis, N.S., P.K. and G.U.K.; investigation, N.S., P.K. and N.S.R.; resources, N.S., G.U.K., P.K. and N.S.R.; data curation, N.S., P.K. and A.B.; writing—original draft preparation, N.S., S.K.T. and M.P.; writing—review and editing, N.S., S.K.T. and M.P.; visualization, N.S., G.U.K. and S.K.T.; supervision, N.S., G.U.K. and S.K.T.; project administration, G.U.K. All authors have read and agreed to the published version of the manuscript.

Funding: This research received no external funding.

Data Availability Statement: Data are contained within the article.

Acknowledgments: The authors are thankful to the management of TATA STEEL Ltd. for their encouragement and support in carrying out the research work and for permission to publish this article.

Conflicts of Interest: Nilamadhaba Sahu, Gajanan U. Kapure, Pankaj Kumar, Sunil Kumar Tripathy, and Arijit Biswas are employees of Tata Steel. The paper reflects the views of the scientists and not the company.

Appendix A

Table A1. Carbothermic reduction of SiO_2 and Al_2O_3 involving the formation of intermediate products, SiO (g), SiC, Al_4C_3, Al_2O (g) [13,18].

Equation Number	Equations
Equation (A1)	SiO_2 (s) + 3C (s) = SiC (s) + 2CO (g); $\Delta G^\circ = 608.97 - 0.340$ T (kJ)
Equation (A2)	SiO_2 (s) + C (s) = SiO (g) + CO (g); $\Delta G^\circ = 688.37 - 0.3388$ T (kJ)
Equation (A3)	$2SiO_2$ (s) + SiC (s) = 3SiO (g) + CO (g); $\Delta G^\circ = 1454.42 - 0.6744$ T (kJ)
Equation (A4)	SiO_2 (s) + Si (l) = 2SiO (g); $\Delta G^\circ = 687.125 - 0.320$ T (kJ)
Equation (A5)	SiO (g) + SiC (s) = 2Si (l) + CO (g); $\Delta G^\circ = 80.169 - 0.03425$ T (kJ)
Equation (A6)	3SiO (g) + CO (g) = $2SiO_2$ (s,l) + SiC (s); $\Delta G^\circ = -1454.42 + 0.6744$ T (kJ)
Equation (A7)	SiO (g) + 2C (s) = SiC (s) + CO (g); $\Delta G^\circ = -81.72 + 0.0011$ T (kJ)
Equation (A8)	2SiO (g) = SiO_2 (s,l) + Si (l); $\Delta G^\circ = -687.12 + 0.320$ T (kJ)
Equation (A9)	$2Al_2O_3$ (l) + 9C (s) = Al_4C_3 (l) + 6CO (g); $\Delta G^\circ = 2438.84 - 1.079$ T (kJ)
Equation (A10)	Al_2O_3 (l) + 2C (s) = Al_2O (g) + 2CO (g); $\Delta G^\circ = 1284 - 0.544$ T (kJ)
Equation (A11)	Al_4C_3 (l) + Al_2O_3 (l) = 6Al (l) + 3CO (g); $\Delta G^\circ = 1593 - 0.672$ T (kJ)

References

1. Sahu, N.; Biswas, A.; Kapure, G.U. A Short Review on Utilization of Ferrochromium Slag. *Miner. Process. Extr. Metall. Rev.* **2016**, *37*, 211–219. [CrossRef]
2. Ashimov, U.; Bolotov, A.; Satvaldiev, D. Using Ferrochromium Slags in the Preparation of Forsterite Refractory. *Refractories* **1984**, *25*, 210–213. [CrossRef]
3. Kumar, P.H.; Srivastava, A.; Kumar, V.; Singh, V.K. Implementation of Industrial Waste Ferrochrome Slag in Conventional and Low Cement Castables: Effect of Calcined Alumina. *J. Asian Ceram. Soc.* **2014**, *2*, 371–379. [CrossRef]
4. Sahu, N.; Biswas, A.; Kapure, G.U. Development of Refractory Material from Water Quenched Granulated Ferrochromium Slag. *Miner. Process. Extr. Metall. Rev.* **2016**, *37*, 255–263. [CrossRef]
5. Zhao, P.; Zhao, H.; Yu, J.; Zhang, H.; Gao, H.; Chen, Q. Crystal Structure and Properties of Al_2O_3-Cr_2O_3 Solid Solutions with Different Cr_2O_3 Contents. *Ceram. Int.* **2018**, *44*, 1356–1361. [CrossRef]

6. Heo, J.H.; Park, J.H. Thermochemical Analysis for the Reduction Behavior of FeO in EAF Slag via Aluminothermic Smelting Reduction (ASR) Process: Part II. Effect of Aluminum Dross and Lime Fluxing on Fe and Mn Recovery. *Calphad* **2017**, *58*, 229–238. [CrossRef]
7. Sarfo, P.; Wyss, G.; Ma, G.; Das, A.; Young, C. Carbothermal Reduction of Copper Smelter Slag for Recycling into Pig Iron and Glass. *Miner. Eng.* **2017**, *107*, 8–19. [CrossRef]
8. Zhang, G.; Wang, N.; Chen, M.; Cheng, Y. Recycling Nickel Slag by Aluminum Dross: Iron-Extraction and Secondary Slag Stabilization. *ISIJ Int.* **2020**, *60*, 602–609. [CrossRef]
9. Halmann, M.; Frei, A.; Steinfeld, A. Carbothermal Reduction of Alumina: Thermochemical Equilibrium Calculations and Experimental Investigation. *Energy* **2007**, *32*, 2420–2427. [CrossRef]
10. *FactSage Software*, FactSage 7.2; CRCT-thermfact Inc. and GTT-technologies: Herzogenrath, Germany, 2018.
11. Baker, D.A.; Siple, J.W. *Methods for the Chemical Analysis of Mineral Chromite and Ferrochrome Slag*; Information Circular 9240; United States Department of the Interior, Bureau of Mines: Washington, DC, USA, 1990; pp. 1–22.
12. Furman, N.H. *Standard Methods of Chemical Analysis*; Forgotten Books: London, UK, 2018; Volume 1.
13. Sakaguchi, Y.; Ishizaki, M.; Kawahara, T.; Fukai, M.; Yoshiyagawa, M.; Aratani, F. Production of High Purity Silicon by Carbothermic Reduction of Silica Using AC-Arc Furnace with Heated Shaft. *ISIJ Int.* **1992**, *32*, 643–649. [CrossRef]
14. Khanna, R.; Kongkarat, S.; Seetharaman, S.; Sahajwalla, V. Carbothermic Reduction of Alumina at 1823 K in the Presence of Molten Steel: A Sessile Drop Investigation. *ISIJ Int.* **2012**, *52*, 992–999. [CrossRef]
15. Ahmed, A.; Faramawy, H.E.; Ghali, S.; Mishreky, M.L. Production of Ferrosilicoaluminium from Aluminum Slag and Local Ore Via Carbothermic Reduction. *Key Eng. Mater.* **2020**, *835*, 75–82. [CrossRef]
16. Yi, S.; Huang, Z.; Huang, J.; Fang, M.; Liu, Y.; Zhang, S. Novel Calcium Hexaluminate/Spinel-Alumina Composites with Graded Microstructures and Mechanical Properties. *Sci. Rep.* **2014**, *4*, 4333. [CrossRef] [PubMed]
17. Braulio, M.; Rigaud, M.; Buhr, A.; Parr, C.; Pandolfelli, V. Spinel-Containing Alumina-Based Refractory Castables. *Ceram. Int.* **2011**, *37*, 1705–1724. [CrossRef]
18. Fruehan, R.; Li, Y.; Carkin, G. Mechanism and Rate of Reaction of Al_2O, Al, and CO Vapors with Carbon. *Metall. Mater. Trans. B* **2004**, *35*, 617–623. [CrossRef]
19. Orlov, A.; Isagulov, A.; Sariev, O.; Tolymbekov, M.Z. Production of Aluminum–Chromium–Silicon Alloy from Unconditioned Materials. *Steel Transl.* **2018**, *48*, 558–563. [CrossRef]
20. Tolymbekov, M.Z.; Akhmetov, A.; Baisanov, S.; Ogurtsov, E.; Zhiembaeva, D. Production and Use of Complex Ferroalloys in Metallurgy. *Steel Transl.* **2009**, *39*, 416–419. [CrossRef]
21. Mekhtiev, A.; Shabanov, Y.; Issagulov, A.; Baissanov, S.; Baissanov, A.; Issagulova, D. Development of Technology of Complex Aluminum-Silicon-Chrome Alloy with Utilization of off Grade Raw Materials. *Metalurgija* **2015**, *54*, 157–160.